Article

Cell Reports

Multiplexed Spike Coding and Adaptation in the Thalamus

Graphical Abstract

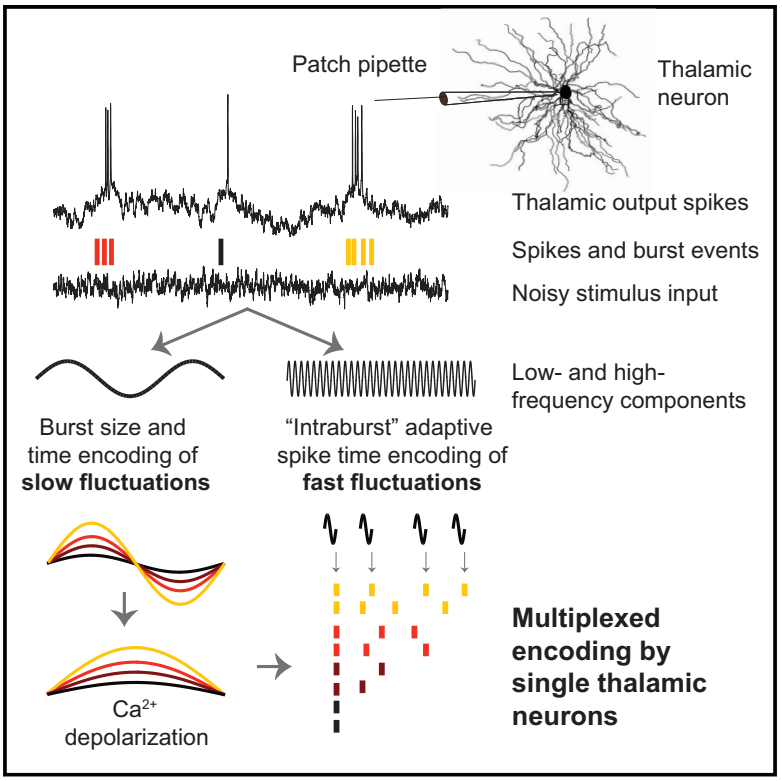

Authors

Rebecca A. Mease, Thomas Kuner, Adrienne L. Fairhall, Alexander Groh

Correspondence

beckin@gmail.com

In Brief

Packets of high-frequency spikes termed "bursts" are a ubiquitous yet enigmatic feature of neural spike trains. Mease et al. investigate computational properties of bursts in the mammalian thalamus, finding that bursts can efficiently encode high- and low-frequency information in parallel. Thus, the cortex may receive more information than previously believed.

Highlights

- Thalamic neurons simultaneously encode high- and low-frequency information
- Precise spike timing within bursts efficiently conveys stimulus details
- Adaptation within bursts makes information transmission robust to contextual change

Mease et al., 2017, Cell Reports *19*, 1130–1140
May 9, 2017
http://dx.doi.org/10.1016/j.celrep.2017.04.050

CellPress

OPEN ACCESS
CellPress

Cell Reports
Article

Multiplexed Spike Coding and Adaptation in the Thalamus

Rebecca A. Mease,[1,2,5,*] Thomas Kuner,[3] Adrienne L. Fairhall,[4] and Alexander Groh[1]
[1]Department of Neurosurgery, Technische Universität München, Munich 81675, Germany
[2]Neurobiology and Behavior Graduate Program, University of Washington, Seattle, WA 98195, USA
[3]Department of Functional Neuroanatomy, Heidelberg University, Heidelberg 69120, Germany
[4]Department of Physiology and Biophysics, University of Washington, Seattle, WA 98195, USA
[5]Lead Contact
*Correspondence: beckin@gmail.com
http://dx.doi.org/10.1016/j.celrep.2017.04.050

SUMMARY

High-frequency "burst" clusters of spikes are a generic output pattern of many neurons. While bursting is a ubiquitous computational feature of different nervous systems across animal species, the encoding of synaptic inputs by bursts is not well understood. We find that bursting neurons in the rodent thalamus employ "multiplexing" to differentially encode low- and high-frequency stimulus features associated with either T-type calcium "low-threshold" or fast sodium spiking events, respectively, and these events adapt differently. Thus, thalamic bursts encode disparate information in three channels: (1) burst size, (2) burst onset time, and (3) precise spike timing within bursts. Strikingly, this latter "intraburst" encoding channel shows millisecond-level feature selectivity and adapts across statistical contexts to maintain stable information encoded per spike. Consequently, calcium events both encode low-frequency stimuli and, in parallel, gate a transient window for high-frequency, adaptive stimulus encoding by sodium spike timing, allowing bursts to efficiently convey fine-scale temporal information.

INTRODUCTION

Complex spiking patterns are a defining property of thalamic neurons and arise from the interplay between fast and slow intrinsic membrane properties. Fast sodium-dependent action potentials (APs) in thalamic neurons can be driven by slow depolarizations resulting from the activation of the T-type calcium current (I_T) (Jahnsen and Llinás, 1984a). I_T availability is tuned by membrane potential, and at physiological extremes, this voltage dependency supports discrete "modes" of spiking: a stimulus may trigger either a single "burst" of high frequency (>100 Hz) APs overlaid on a low-threshold calcium spike (LTS) or a train of regular "tonic" APs when I_T is unavailable.

This complex intrinsic property is common to all thalamic systems (Llinás and Steriade, 2006), and the characteristics of I_T appear to be evolutionarily conserved and subject to significant functional constraints (Senatore et al., 2012). However, despite the ubiquity of this markedly nonlinear behavior, the functional role of thalamic bursting is not understood. Early studies of thalamic information processing largely focused on the difference between the two spiking modes, suggesting that thalamic bursting may not encode any information and instead indicates a state of "sensory uncoupling" (Coenen and Vendrik, 1972; Livingstone and Hubel, 1981) or serves as a strong but unspecific "wake-up call" to the cortex, while tonic spiking serves to encode fine stimulus details (Sherman, 2001).

More recently, this strict burst/tonic functional dichotomy has been rejected with the widespread observation of burst spiking in awake animals (Ramcharan et al., 2000; Fanselow et al., 2001; Martinez-Conde et al., 2002; Weyand et al., 2001; Swadlow and Gusev, 2001). Furthermore, in vivo studies in the cat primary visual thalamus have demonstrated that thalamic bursts can convey significant information about sensory inputs (Guido and Weyand, 1995; Weyand et al., 2001; Reinagel et al., 1999; Martinez-Conde et al., 2002), particularly in response to stimuli with naturalistic spatiotemporal structure and correlation (Wang et al., 2007; Lesica and Stanley, 2004; Denning and Reinagel, 2005; Lesica et al., 2006; Alitto et al., 2005). Thalamic neurons also adapt in response to ongoing stimulation (Simons and Carvell, 1989; Maravall et al., 2013; Lesica et al., 2007), and control of adaptation has been associated with modulation of bursting (Mease et al., 2014; Whitmire et al., 2016; Wolfart et al., 2005).

Much of the progress in understanding how thalamic spiking patterns encode information has been made by characterizing in vivo responses to complex, naturalistic stimuli in intact circuits using reverse correlation (de Boer and Kuyper, 1968), linear-nonlinear modeling (Korenberg and Hunter, 1986), and/or information theoretic methods (Butts et al., 2010; Alitto et al., 2005; Lesica et al., 2006, 2007; Lesica and Stanley, 2004; Reinagel et al., 1999; Maravall et al., 2013; Petersen et al., 2008; Gaudry and Reinagel, 2008; Denning and Reinagel, 2005). These studies have shown that compared to tonic spikes, burst onset timing carries distinct sensory information (Reinagel et al., 1999; Alitto et al., 2005; Lesica et al., 2006; Lesica and Stanley, 2004; Denning and Reinagel, 2005) and that the number of spikes in a burst (Gaudry and Reinagel, 2008) or spiking "episode" (Butts et al., 2010) can carry additional information. In combination with the known intrinsic properties of thalamic neurons, these studies

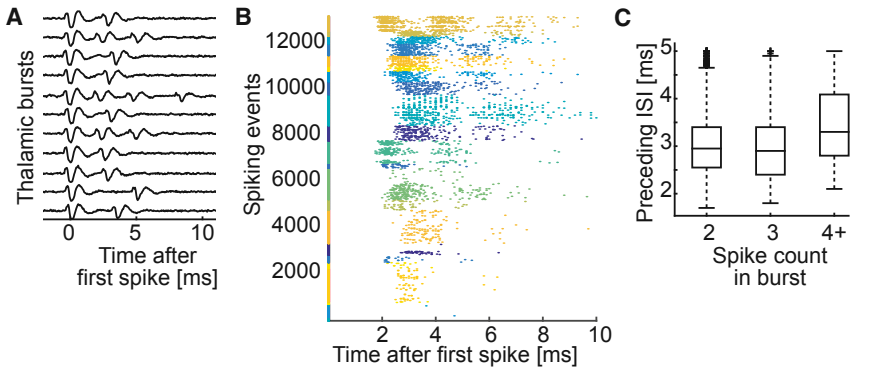

Figure 1. Variation in Thalamic Spiking Events In Vivo

(A) Example thalamic burst recording in vivo from a juxasomally recorded POm thalamic neuron in a urethane anesthetized mouse. Here, thalamic spikes are driven by spontaneous cortical inputs from layer 5 in the barrel cortex as described in Mease et al. (2016c).

(B) POm spiking event rasters for a group of POm in vivo recordings triggered on the first spike in a burst (n = 23 neurons, different colors) pooled from 11 animals.

(C) ISIs sorted by spike order, pooled across neurons shown in (B).

predict that thalamic stimulus encoding is largely shaped by I_T. However, the systems-level advantage of in vivo preparations—the ability to map spiking patterns to peripheral sensory inputs—also makes it difficult to disambiguate circuit and single-neuron properties, experimentally control the precise statistics of currents driving the neuron of interest, or manipulate biophysical properties. Therefore, questions regarding intrinsic information processing in single neurons are currently most tractable using in vitro methods.

Recent in vitro studies have provided richer understanding of the biophysical properties supporting bursting, demonstrating that I_T is active at depolarized resting potentials seen in the awake state (Bessaïh et al., 2008; Lambert et al., 2014; Dreyfus et al., 2010) and also contributes to presumed "tonic" spiking patterns (Deleuze et al., 2012). However, despite agreement between in vitro and in vivo lines of evidence that thalamic information processing is more nuanced than binary switches between tonic and burst output modes, it is unknown how features of synaptic inputs are encoded by thalamic bursts.

In the present study, we use direct current injection into single neurons along with manipulation of channel dynamics to evaluate how the intrinsic properties of thalamic neurons shape their coding properties. We apply in vitro reverse correlation and linear-nonlinear modeling in rodent thalamic neurons of the posterior medial thalamic nucleus (POm) using whole-cell patch-clamp recordings and Gaussian noisy current stimulation. POm is a "higher-order" thalamic nucleus in the whisker system that receives diverse and well-characterized synaptic inputs, including powerful excitatory inputs from layer 5B (L5B) of barrel cortex (Groh et al., 2008, 2014; Reichova and Sherman, 2004; Mease et al., 2016c; Sherman and Guillery, 2006). For a subset of experiments, we used the presence of these L5B inputs to precisely target neurons in the POm (Groh et al., 2008). These approaches allowed us to quantify thalamic single-neuron computation in isolation from network-level effects while limiting assumptions about input statistics. We could then quantify how characteristics of the input current are encoded by different properties of thalamic bursts and relate this code to underlying biophysical mechanisms.

We begin by framing the issue of burst encoding using in vivo POm data illustrating that thalamic bursts are not uniform (see also Reinagel et al., 1999; Wang et al., 2007; Martinez-Conde et al., 2002; Gaudry and Reinagel, 2008) and vary with respect to size, frequency, and spike timing within burst events. We next establish our in vitro analysis approach by comparing the classic burst and tonic modes in the linear-nonlinear model framework and with information theoretic methods. Our preparation allows us to study the encoding properties of thalamic bursts at a higher level of detail than in previous work and to determine how intrinsic thalamic adaptive properties change the encoding as the statistical context of the current stimulus varies.

Our first main result is that bursts convey an unexpected level of stimulus detail via multiple channels: the times and sizes of burst events and, most strikingly, the precise timing of APs within bursts as well. These data show that thalamic neurons employ multiplexed stimulus encoding in that bursts can simultaneously encode both high- and low-frequency information. The second main result is that burst onset initiates a brief period of efficient encoding in which adaptation normalizes AP initiation according to background fluctuations. These findings suggest that the post-synaptic cortical targets of thalamic neurons may have access to a far richer, more dynamic description of synaptic inputs than has been assumed to date, and they show how many characteristics of thalamic computation measured at the circuit level arise from the intrinsic properties of single thalamic neurons.

RESULTS

In vivo, spontaneous cortical oscillations drive POm thalamic neurons to spike without application of additional stimuli (Groh et al., 2014; Mease et al., 2016c) (Figure 1). Figure 1A shows an example recording of POm bursts and Figure 1B a group of such recordings reported previously (Mease et al., 2016c). Spiking events are non-uniform, in that bursts can contain a variable number of spikes, and for each neuron, the timing of successive spikes varies between events. The distribution of successive interspike intervals (ISIs) (Figure 1C) shows that ISIs vary over a window of more than 3 ms, even when spike order is taken into consideration. Our goal here is to determine how these features of bursts encode underlying synaptic inputs.

Understanding how variation in neural responses encodes properties of the sensory scene or synaptic input currents is a natural application for information theoretic approaches (Rieke et al., 1997; Shannon and Weaver, 1963), and these methods

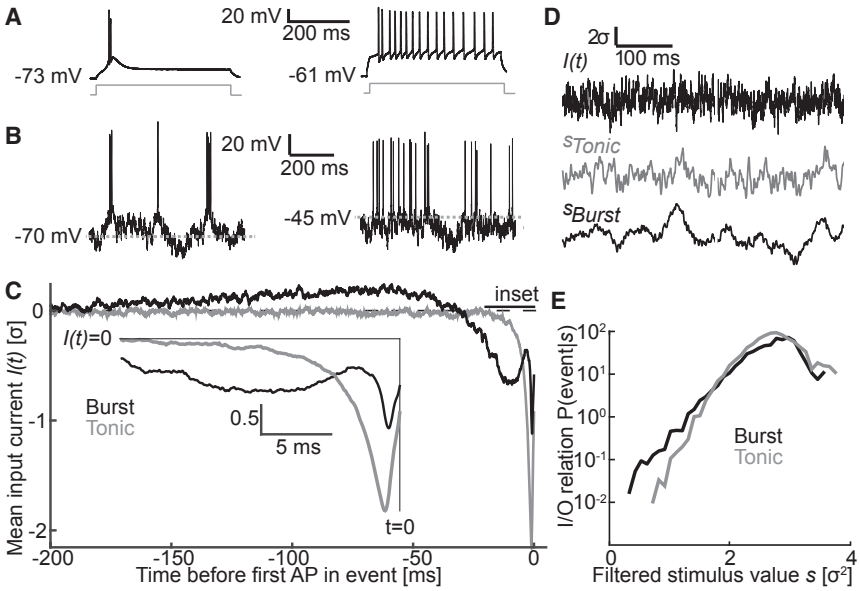

Figure 2. In Vitro Noise-Evoked Firing in Thalamic Neurons Reveals Feature Selectivity on Different Timescales

(A and B) Whole-cell in vitro patch-clamp recording of a POm neuron illustrates burst (left) and tonic (right) mode firing in response to (A) current step (250 pA) or (B) noise stimuli.

(C) Event-triggered average (ETA) stimuli for a representative POm neuron. Depolarization transitions ETA shape from a two-peaked biphasic (black) to a simpler monophasic (gray) shape. Similar results were seen in all neurons (n = 7 neurons recorded in both burst and tonic modes and n = 8 additional neurons recorded only in burst mode).

(D) Filtering the raw input stimulus I(t) (top) by the ETAs shown in C preserves high-frequency oscillations in the tonic case (s_{tonic}, middle) and slow oscillations and small high-frequency oscillations in the burst case (s_{burst}, bottom).

(E) Input/output relations for tonic and burst ETAs shown in (C). These functions relate the value of the filtered stimuli shown in (E) to the probability of generating a spiking event. Slopes fit to log-linear portion of IO relations for this neuron were 1.5 and 2.3 (units of $\log_{10}$ event probability/σ^2) for burst and tonic modes, respectively.

See also Figures S1–S3.

have been applied to thalamic spike trains recorded in vivo (e.g., Gaudry and Reinagel, 2008; Butts et al., 2010; Denning and Reinagel, 2005). Information theory allows one to quantify how knowledge of a given neural response (e.g., the number of spikes in a burst, or the timing of a spike) reduces uncertainty—mathematically, the entropy of the distribution—about the stimulus (e.g., motion of a whisker, or the net synaptic current). This reduction in uncertainty is the information carried by the response about the stimulus and is commonly measured in bits; each bit of information indicates a 2-fold decrease in uncertainty.

Averaging across the group of in vivo recordings in Figure 1, the entropy of burst size is 0.77 ± 0.47 bits, and the spike-timing entropy of spikes within bursts is 1.9 ± 1.0 bits (time bin = 0.4 ms). These variable quantities are channels by which thalamic spiking events can possibly encode information. Motivated by these in vivo observations of burst variability, we next investigate how information about complex inputs can be encoded by the properties of POm bursts in a controlled in vitro setting.

Noise Stimulation of Thalamic Neurons

As is characteristic of all thalamic relay neurons, POm neurons in brain slices respond to depolarizing current steps (Figure 2A) with either high frequency (>100 Hz) "bursts" of APs when hyperpolarized or regular "tonic" APs when depolarized (Jahnsen and Llinás, 1984a; Landisman and Connors, 2007). In burst mode, sodium APs are overlaid on an LTS, the slow (~50 ms) depolarization arising from activation of the transient low-threshold calcium current I_T.

To understand how complex, time-varying stimuli are encoded during these two spiking modes, we measured the intrinsic stimulus encoding of POm neurons during stimulation with broadband Gaussian "noise" current (Figure 2B). Neurons responded with complex AP patterns in each mode, but the overall spiking modes were maintained. In burst mode, responses consisted of clusters of APs overlaid on slow LTS depolarizations (Figure 2B, left), with burst events consisting of two or more APs accounting for more than half of all events (38% ± 21%, 29% ± 9%, 18% ± 9%, and 15% ± 21% for event sizes of one, two, three, or four or more APs, respectively; n = 15). In contrast, in tonic mode, neurons produced APs at irregular intervals in response to the same current waveform (Figure 2B, right). The cumulative ISI distributions reflect these distinct patterns (Figures S1A and S1B). In the following, we refer to either single APs or bursts of APs as "spiking events."

Slow and Fast Timescales of Thalamic Intrinsic Computation

We characterized the intrinsic computation of each thalamic neuron as a linear-nonlinear cascade (Figures 2C–2E) consisting of (1) a spike-triggering current feature and (2) a measure of sensitivity to that feature, mapping input stimuli to output spiking events. These two model components quantify the temporal pattern of input current that trigger APs and the relative selectivity the neuron has for this pattern. From the responses to noise, we calculated the relevant feature as the "event-triggered average" (ETA) current by triggering on either the first AP in a burst spiking event or single APs in tonic mode. The ETA shows the combination of current inputs that on average are most successful in driving spiking events.

ETA_{Tonic} (Figure 2C, gray) was a relatively brief depolarizing current, indicating that tonic APs were generated by a sharp monophasic depolarization within a 10 ms window. This

ETA_{Tonic} is similar in form to ETAs measured in cortical neurons (e.g., Mease et al., 2013). In contrast, the burst mode ETA_{Burst} (Figure 2C, black) had a more complex biphasic shape and long integration window, combining (1) a slow (~200 ms) oscillation consisting of a hyperpolarizing current followed by a broad depolarizing current and (2) a very fast (<5 ms) oscillation consisting of a brief hyperpolarizing current followed by a sharp depolarization immediately preceding the AP. This "compound" shape resembles the sum of two separate ETAs with long and short integration windows.

Thus, the AP-triggering feature space changes dramatically in timescale and amplitude between burst and tonic modes, particularly with regard to the range of stimulus frequencies encoded. We project the raw current stimulus $I(t)$ into the dimensions defined by ETA_{Burst} and ETA_{Tonic} (Figure 2D) by finding the vector dot product between each feature and the stimulus preceding each spiking event. This procedure gives filtered stimuli s_{Burst} and s_{Tonic}, which measure the similarity between the raw stimuli and the ETAs. The two spiking modes enhance distinct frequency components of the stimulus (Figure S1C): in tonic mode, intermediate frequencies are retained in s_{Tonic}, while in burst mode, very low and very high frequencies are emphasized in s_{Burst} due to the compound "slow-fast" shape of ETA_{Burst}. In contrast to previous analysis of the filtering properties of visually evoked tonic spikes and bursts (Lesica and Stanley, 2004), the preservation of high frequencies in s_{Burst} suggests that the timing of burst events can simultaneously encode fast and slow stimulus patterns.

The ETAs quantify which patterns of stimuli are encoded in thalamic spiking events at different membrane potentials but do not indicate how selective the neuron is for these patterns (i.e., how closely the input must match the ETA for a spiking event to occur). To further examine the changes in information encoding between tonic and burst mode, we quantified how different values of filtered stimuli s_{Burst} and s_{Tonic} map to the occurrence of spiking events (Figure 2E) by sampling input-output (IO) relations $P(event|s_{Burst})$ and $P(event|s_{Tonic})$ (see Experimental Procedures). Neurons in tonic mode encoded current stimuli more precisely across a narrower dynamic range, as the slope of $P(event|s_{Tonic})$ was greater than that of $P(event|s_{Burst})$ by a factor of approximately two (median slopes were 1.2 [interquartile range [IQR] = 1.1–1.5] and 2.4 [IQR = 2.2–2.7] for burst and tonic IO relations, respectively; $p < 0.05$ two-tailed Wilcoxon rank sum test; data pooled from seven neurons recorded in both firing modes). This finding is in agreement with Wolfart et al. (2005), who found that hyperpolarization and concomitant increase in I_T availability broadened thalamic IO relations. However, given that the two spiking modes show very different responses to identical stimuli (Figure 2B), this change in IO relation was not as dramatic as might be expected; most of the difference in computation was captured by the change in the shape of the ETA (Figure 2C).

Repeated presentation of a noisy stimulus allowed us to calculate how much information about the stimulus was encoded by the timing of burst and tonic spiking events (Supplemental Experimental Procedures; Figure S2; Fairhall et al., 2006; Brenner et al., 2000; see Gaudry and Reinagel, 2008; Denning and Reinagel, 2005; Reinagel et al., 1999 for related analysis in the visual thalamus). Burst events were typically at least 2 bits more informative about the stimulus than were tonic events (Figures S2A and S2B), in agreement with Reinagel et al. (1999) and previous reports that burst events are more precise than tonic spikes (Zeldenrust et al., 2013; Whitmire et al., 2016; Kepecs and Lisman, 2003). We next calculated I_{fract}, the fraction of information captured by the ETA (Fairhall et al., 2006). I_{fract} for ETA_{Tonic} reached a maximum of ~70% at smaller (1–1.5 ms) dt, whereas I_{fract} for ETA_{Burst} reached a maximum of ~55% at larger (10–12 ms) dt (Figure S2C). I_{fract} in burst mode was also nonzero for dt <10 ms, indicating that burst spiking events also carried high-frequency information, consistent with the filtering properties of ETA_{Burst} (Figures 2C and 2D). Notably, maximum I_{fract} was always less for burst mode than for tonic mode, suggesting that the linear-nonlinear (LN) model characterization using burst spiking events as stereotyped "unitary" events failed to capture some aspect of stimulus encoding in burst mode. We next examine this discrepancy in more detail by considering the role of AP count within bursts.

Properties of Bursts Convey Different Types of Information

The disparity in timescales between the ETAs (Figure 2C) matched the difference in kinetics between the voltage-gated sodium and calcium currents controlling excitability in thalamic neurons. Burst mode is controlled by the voltage-dependent availability of both I_T and I_{Na}, while during tonic mode, I_T is mostly inactivated due to depolarization (Jahnsen and Llinás, 1984a, 1984b). As depolarization simplifies the structure of ETA_{Burst} from a biphasic current to a single more generic depolarizing current, the slow timescales most likely arise from the kinetics of I_T (Jahnsen and Llinás, 1984a). Indeed, the application of the I_T channel blocker mibefradil (Figure S3) had a similar effect on the ETA as depolarization. Together, these experiments demonstrate that the slow oscillatory ETA_{Burst} shape reflects initial deinactivation (hyperpolarizing lobe) and subsequent activation (depolarizing lobe) of I_T.

Thus, the slow component of ETA_{Burst} can be thought of as triggering an I_T-dependent LTS, while the fast component determines the precise timing of the leading sodium AP in a burst. To examine these two channels separately, we decomposed ETA_{Burst} as a linear combination of two separate dimensions (Figures 3A and S4A): (1) slow ETA_{Ca}, and (2) fast ETA_{Na} (see Experimental Procedures). Measured as I_{fract} of the total information carried by spiking event times (Figure 3B), ETA_{Ca} or ETA_{Na} individually captured less information than the compound feature ETA_{Burst}, but taken jointly, it captured more total information, especially at short timescales. However, it should be noted the information calculated jointly may be artificially high, as ETA_{Ca} and ETA_{Na} are not orthogonal, although nearly so (see Experimental Procedures).

The utility of this decomposition is seen when considering bursts of different sizes (Figure 3C). Here, we ignore the precise timing of APs within a burst and treat bursts as single events with different AP counts, which typically varied between one and five APs per spiking event. To illustrate the motivation behind this analysis, we calculated the compound ETA_{Burst} separately for bursts with different AP counts (Figure S4B); larger bursts are

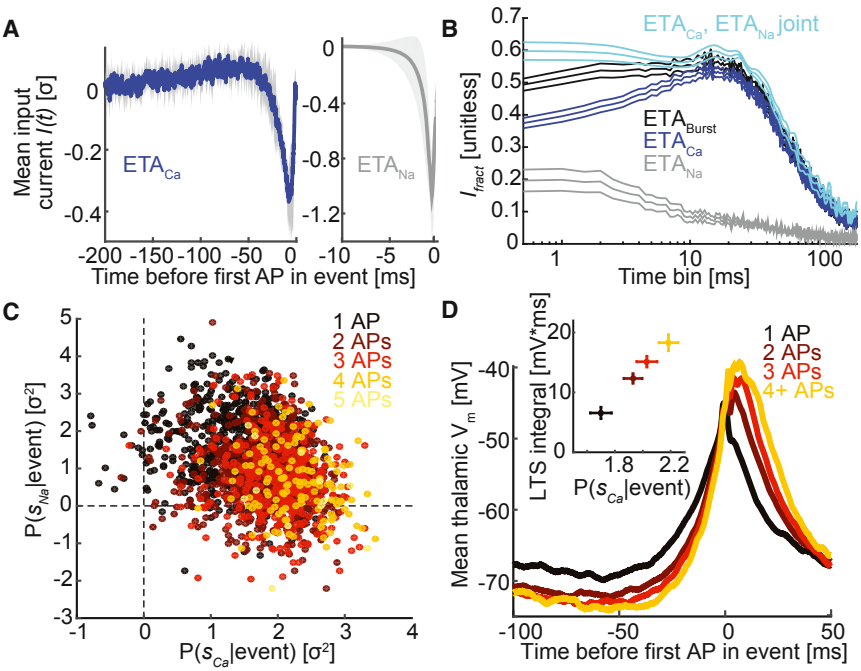

Figure 3. Sodium and Calcium Spike-Triggering Features Are Separable in Burst Mode

(A) Burst mode ETAs separated into slow calcium ETA_{Ca} (left, blue) and fast sodium ETA_{Na} (right, gray) components (see Experimental Procedures and Figure S4). Population means shown; note 10 × difference in timescale.

(B) Information capture fraction I_{fract} versus bin size for the compound burst ETA (black), the single features ETA_{Ca} (blue) and ETA_{Na} (gray) from (A), and the joint representation in ETA_{Na} and ETA_{Ca} (cyan); values plotted are population means ± SEM (n = 7 neurons).

(C) Event-triggering stimuli projected into s_{Na} (ordinate) and s_{Ca} (abscissa) space. Each marker shows one spiking event; color indicates AP count per event. Correlation coefficient between $s_{Ca}|event$ and $s_{Na}|event$ for this neuron was −0.27.

(D) Event-triggered average voltage by AP count for a representative POm neuron. To emphasize slow fluctuations, spikes were truncated using a median filter (window size = 2.5 ms). Inset: integral of LTS from −50 ms to 50 ms versus the average s_{Ca} before each spiking event (population mean n = 15) for different sized bursts; error bars show mean ± SD each dimension. Color conventions as in (C).

See also Figure S4.

preceded by a larger slow oscillation and a smaller fast oscillation. To quantify how ETA_{Na} and ETA_{Ca} stimulus features are encoded in thalamic AP trains, we project the raw stimulus $I(t)$ into a two-dimensional space of s_{Na} versus s_{Ca} (Figure 3C). We then parse the burst-size-dependent change in feature selectivity into the simplified dimensions of ETA_{Ca} and ETA_{Na} by examining how the joint event-triggering stimulus distribution P $(s_{Na}, s_{Ca}|event)$ changes as a function of spiking event size.

Most importantly, s_{Ca} was highly predictive of output AP count (event size). Figure 3C shows P $(s_{Na}, s_{Ca}|event)$ for a representative recording. Each marker represents one spiking event (e.g., a single AP or a burst of two or more APs), colored according to the number of associated sodium APs. Within this two-dimensional space, the event-triggering stimulus distribution shifts according to event size: as event size increases, s_{Ca} increases and s_{Na} decreases. P $(s_{Na}|event)$ and P $(s_{Ca}|event)$ were negatively correlated for all neurons (mean $r = -0.25 \pm 0.11$; n = 15). Figure S4C summarizes this tradeoff versus event size; for spiking events with only one sodium AP, fast and slow frequencies were equally important, but as AP count increased, the importance of the slow feature dominated.

We interpret these data as showing that LTSs that trigger more sodium APs encode more information about the slow feature and are triggered by larger slow oscillations (i.e., larger s_{Ca}), and that the precise time of the first sodium AP in such large events is less dependent on high-frequency fluctuations (i.e., smaller s_{Na}). We quantified information I_{ETA} captured by ETA_{Na} and ETA_{Ca} as a function of burst size (Figure S4D) by examining how the distributions of s_{Ca} and s_{Na} changed as a function of AP count (Supplemental Experimental Procedures). This approach showed a comparable trend: bursts of increasing AP count encoded more information about the slow feature ETA_{Ca} ($I_{ETA} = 2.4 \pm 0.2$, 3.3 ± 0.2, and 3.7 ± 0.2 bits for AP counts of one, two, and three or more, respectively; bin size = 0.2 σ; mean ± SEM for n = 7 neurons), whereas information about the fast feature ETA_{Na} was greatest for spiking events with only one AP ($I_{ETA} = 2.4 \pm 0.4$, 1.1 ± 0.3, and 1.1 ± 0.4 bits for AP counts of one, two, and three or more, respectively; bin size = 0.2 σ; mean ± SEM for n = 7 neurons).

While the LTS slow depolarization is often referred to as a "spike," the shape of the LTS is not always stereotyped. Instead, the amplitude and duration of the LTS are strongly dependent on membrane potential history, as seen in the original report by Jahnsen and Llinás (Jahnsen and Llinás, 1984a). In our case, stimulation with a complex noise current evoked LTSs with variable amplitude. LTS amplitude was positively correlated with s_{Ca}, the projection onto the slow ETA_{Ca}. We quantified the LTS by calculating the average event-triggered membrane potential (Figure 3D), which showed a clear progression in the shape of the LTS as a function of the number of APs: greater numbers of sodium APs are associated with larger LTSs that (1) were preceded by more hyperpolarization and had (2) longer duration, (3) greater amplitude, and (4) a faster rate of rise. These last two points predict that, as we observed, fast fluctuations are less important to initial spiking, for the following reasons: more boosting depolarization from the LTS ensures precise AP timing regardless of additional high-frequency inputs, and a faster rate of rise ensures a lower sodium activation threshold due to decreased fast sodium channel inactivation during the approach to threshold. In fact, there was a very clear correspondence between the value of s_{Ca} and the size of the resultant LTS (Figure 3D, inset), which is consistent with larger s_{Ca} being associated with greater numbers of APs.

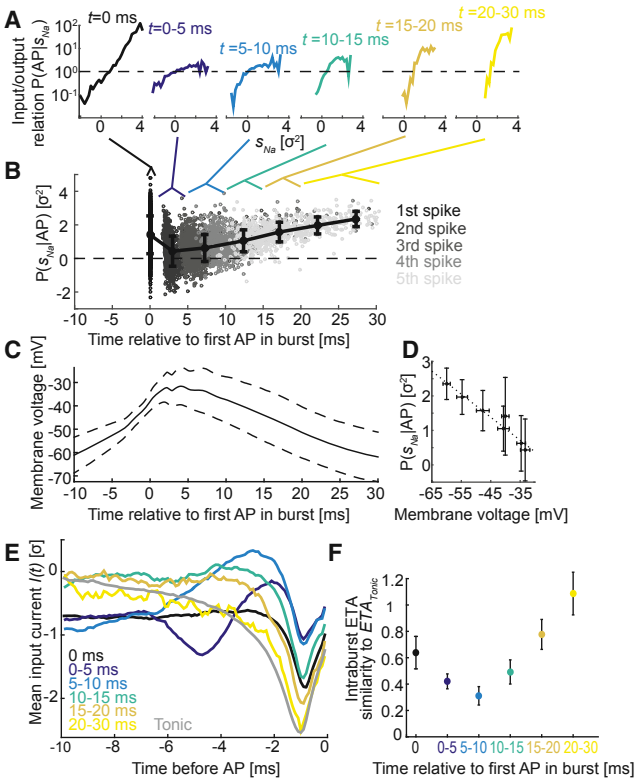

Figure 4. Voltage-Dependent High-Frequency Selectivity throughout Bursts

(A and B) IO relation $P(AP \mid s_{Na}, t)$ for sodium APs (A) evolves throughout multiple AP bursts (colored by time window) due to the changing distribution of $s_{Na}|AP$ (B). Each marker in (B) shows s_{Na} for one AP as a function of time from the first AP in the burst; black to gray indicates increasing AP order. Black open markers show mean of $s_{Na}, t|AP$ for the initial AP in a burst (t = 0) and t = 5 ms bins thereafter.

(C) Mean LTS depolarization for the same neuron and same timescale.

(D) Mean $s_{Na}, t|AP$ from B plotted versus corresponding mean binned membrane potential at t in (C), showing strong correlation between $s_{Na}|AP$ and the shape of the underlying LTS.

(E) Progression of intraburst ETA_t throughout a burst; color code indicates same AP binning categories as in (A). Gray trace is ETA_{Tonic} for the same neuron.

(F) Similarity of ETA_{Tonic} to intraburst ETA_t s shown in (E), calculated as the vector dot product. Each data point shows mean and SD for n = 7 neurons with both tonic and burst conditions; color code as in (A) and (E).

High-Frequency Stimulus Encoding by APs within Bursts

The presence of the high frequency component ETA_{Na} shows that the timing of the initial AP in a burst is sensitive to particular stimulus patterns and not simply triggered by the LTS depolarization. This finding suggests that subsequent "intraburst" APs in a burst might also encode particular stimulus features. This possibility is important because thalamic bursts have been regarded as inflexible, stereotyped events that signal the occurrence of environmental change (Sherman and Guillery, 2006), rather than conveying detailed information about the stimulus in the specific temporal patterns of spikes. In contrast to our previous treatment of bursts of APs as single events in Figure 3, we next found LN models as a function of AP time *within* bursts (Figure 4) by calculating the values of high-frequency stimuli s_{Na} which drove intraburst APs.

In the case that the timing of intraburst APs depends only on the underlying LTS depolarization, the distribution of event-triggering high-frequency stimuli $P(s_{Na}|event)$ for these APs should be identical to $P(s_{Na})$, creating a flat IO relation. Contrary to this expectation, $s_{Na}|event$ for intraburst APs was on average positive, indicating intraburst selectivity for high-frequency inputs. Furthermore, the selectivity for high frequencies varies as a function of time relative to the initial AP in a burst. This result comes from examining how the distribution of s_{Na} for intraburst APs changes for successive APs (i.e., finding $P(s_{Na}, t|event)$, where t is time relative to the first AP in a burst).

Figure 4 shows the time-resolved selectivity for s_{Na} throughout a burst, with IO relations $P(event \mid s_{Na}, t)$ in (Figure 4A) and the corresponding values of s_{Na} plotted versus time t relative to initial AP in a burst event (Figure 4B). Values of s_{Na} are shaded according to AP order in the burst, and the black overlay shows mean s_{Na} value plotted by mean t within 5 ms intervals. In a case where ETA_{Na} is entirely irrelevant to the generation of APs and APs are driven only by the underlying LTS depolarization, the IO relations $P(event \mid s_{Na}, t)$ (Figure 4A) would be flat (dotted lines), and the corresponding projections (Figure 4B) would be centered at zero with an SD of one. Contrary to these expectations, mean s_{Na} values were always positive and showed a distinctive progression throughout the course of the burst, indicating that throughout a burst, intraburst AP timing becomes increasingly dependent on ETA_{Na}, increasing the slope of $P(event \mid s_{Na}, t)$. (Figure 4A). For subsequent APs occurring ~2–7 ms after the first AP, the importance of high frequencies is at a minimum but steadily increases for APs occurring later in the burst, with mean s_{Na} reaching a maximum for the latest APs.

What causes this progression in selectivity for high frequencies? We found that the time course of selectivity (Figure 4B) for ETA_{Na} was tightly linked to the depolarization from the LTS (Figure 4C). Replotting the mean s_{Na} value by membrane potential during segments of the LTS (Figure 4D) revealed a strong linear relationship between high-frequency selectivity (mean s_{Na}) and depolarization (correlation coefficient $r = -0.84 \pm 0.22$, n = 15 neurons). Taken together, these observations suggest that while initial APs may be mostly dependent on the underlying LTS calcium event, later APs are increasingly sensitive to high-frequency inputs that occur while the LTS decays. Thus, the ETA_{Ca} stimulus feature that drives the LTS shifts the neuron into a transient regime of selectivity for fast stimulus features similar to ETA_{Na}.

To illustrate this point in an alternative but complementary way, we plot ETA_t triggered on APs from different periods t within a burst (Figure 4E). The waveform correlated to initial APs in a burst is ETA_{Na} and is a simple depolarizing transient; in contrast, intermediate APs at the peak of the LTS are driven by smaller depolarizing transients preceded by brief hyperpolarization. Finally, for later APs, the ETAs simplify and become increasingly similar to ETA_{Tonic} for the same neuron. We quantify similarity between tonic and intraburst ETAs and see the same progression (Figure 4F) across all neurons. This finding directly demonstrates the changing importance of high-frequency stimulus components during the course of the LTS and suggests that intraburst

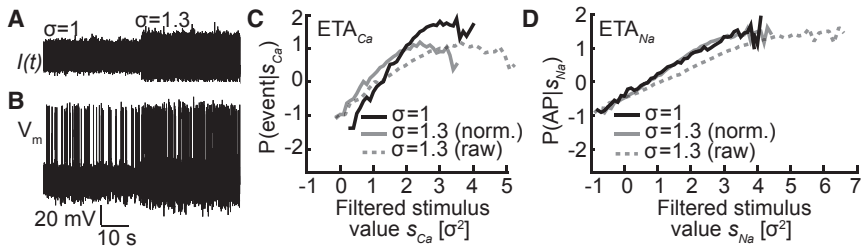

Figure 5. Different Adaptive Characteristics of Sodium and Calcium Feature Selectivity

(A) Example input current stimulus, SD (σ) switching at 40 s intervals from σ = 1 to σ = 1.3.

(B) Sample POm voltage response.

(C and D) IO relations for calcium (C) and sodium (D) events, for raw stimulus values (black, σ = 1; solid gray, σ = 1.3 normalized; gray dashed, σ = 1.3 unnormalized). Gain scaling error was more than 6-fold greater for ETA_{Ca} than ETA_{Na} (1.9 ± 0.65 and 0.3 ± 0.08 bits, for slow and fast features, respectively, see Experimental Procedures).

See also Figure S5.

encoding is comparable to the purely tonic firing regime, particularly for initial and later APs, which do not receive maximal depolarizing drive from the LTS. These high frequencies have not been explicitly represented in previous in vivo work, where visual stimuli typically varied more slowly than the noise current used here.

These data demonstrate that the information coding capacity of thalamic bursts is contained not only in the burst onset time or total AP count but also in the precise timing of APs within a burst. This simultaneous encoding of distinct stimulus characteristics is an example of "multiplexing," a strategy that greatly enhances the coding efficiency of single neurons (Fairhall et al., 2001; Panzeri et al., 2010).

Adaptation in High- and Low-Frequency Information Channels

Adaptation to sustained stimulation is a key computation in the rodent somatosensory system (Maravall et al., 2007, 2013; Whitmire et al., 2016), and given the complex intrinsic feature selectivity of thalamic neurons we report here, we hypothesized that these computational properties might support adaptation at the level of single cells (Mease et al., 2013). To determine if and how POm stimulus encoding adapts to shifts in statistical context, we switched the SD (σ) of the stimulus (Figures 5A, 5B, and S5A–S5C) and compared LN models across σ conditions (Figures S5D–S5G, 5C, and 5D). The fast ETA_{Na} and slow ETA_{Ca} channels showed very different adaptive responses, in that changing σ altered the essential shape of the event-triggering currents encoded by slow LTS events, but not fast sodium APs (Figures S5D–S5G).

Most importantly, for the fast feature ETA_{Na}, the IO relation had the same fundamental shape, regardless of σ. An increase in σ decreased the slope and increased the dynamic range of both $P(event \mid s_{Ca})$ (Figure 5C) and $P(event \mid s_{Na})$ (Figure 5D). However, when re-expressed in normalized units, this difference disappeared for $P(event \mid s_{Na}/\sigma)$ (Figure 5D). This property is a hallmark of adaptive "gain scaling" behavior (Fairhall et al., 2001; Maravall et al., 2007; Mease et al., 2013), in which a neuron's excitability adjusts precisely to maintain the same information encoded per AP, regardless of the overall statistical context. In marked contrast, the normalized IO relations $P(event \mid s_{Ca}/\sigma)$ retained the σ-dependent decrease in selectivity. Thus, both the slow ETA feature and the neurons' sensitivity to that feature depend on the statistical context of the stimulus. We conclude that stimulus encoding by sodium APs and calcium LTSs adapts differently with respect to changes in stimulus context.

DISCUSSION

Thalamic Multiplexing

We find that the contribution of I_T to thalamic excitability and bursting initiates a transient but efficient period of stimulus encoding: an initial selectivity for slow inputs by I_T-mediated LTSs and subsequent variance-independent selectivity for fast inputs by sodium APs. This finding suggests a role for bursts in transmitting fine stimulus details, a function that was largely assigned to the tonic thalamic relay mode.

At voltages with available I_T, thalamic spiking events encode three types of information: (1) the timing of a spiking event indicates the occurrence of a slow oscillation (Figure 2), (2) the number of APs generated during a spiking event indicates the amplitude of this slow oscillation (Figure 3), and most strikingly, (3) the precise timing of APs within a spiking event encode the timing of very fast oscillations (Figure 4). This encoding scheme is an example of a multiplexed code in which both overall spike count and spike timing carry information (Fairhall et al., 2001; Panzeri et al., 2010) and reveals that the raw information coding capacity of thalamic neurons is far greater than previously reported.

Burst and Tonic Feature Selectivity

To establish our analysis framework, we show that burst and tonic spiking events encode very different patterns of current (Figure 2C). This finding is agreement with studies in the visual thalamus showing that bursts evoked by noisy or natural scene stimuli are triggered by periods of inhibitory visual stimuli followed by excitatory visual stimuli integrated over hundreds of milliseconds, whereas single tonic spikes are evoked by visual stimuli favoring excitation within 100 ms of the spike (Alitto et al., 2005; Butts et al., 2010; Wang et al., 2007; Gaudry and Reinagel, 2008; Lesica and Stanley, 2004; Lesica et al., 2006; Reinagel et al., 1999). We find that this circuit-level feature encoding can occur on the level of membrane potential dynamics of single thalamic neurons, as the slow component (ETA_{Ca}) of ETA_{Burst} had a temporally broad (>200 ms), biphasic shape (Figure 2C), integrating temporally offset inhibitory and excitatory currents, whereas ETA_{Tonic} was only excitatory and had a comparatively brief integration window. We predict that the overall balance between slow modulatory excitatory and inhibitory inputs to POm (Sherman and Guillery, 2006) would serve to fix the shape of the event-triggering stimulus feature between the extremes of ETA_{Burst} and ETA_{Tonic} (Figure 2C) via slow changes in membrane potential and the consequent availability of I_T.

In contrast to these previous studies, the fast component (ETA_{Na}) of ETA_{Burst} demonstrates that burst onset timing can also encode high-frequency stimuli in addition to slower inhibitory and excitatory inputs. Relatedly, we find that the integration window of ETA_{Tonic} is much shorter (<10 ms) than comparable measures reported previously (Lesica and Stanley, 2004; Alitto et al., 2005; Wang et al., 2007). The most obvious explanation for these differences is that our in vitro experiments allowed us to directly test the contribution of higher-frequency current to thalamic AP generation, beyond the temporal resolution possible in previous approaches using sensory rather than current stimulation. Another possible explanation for the fast timescale we observe in ETA_{Tonic} is that our manipulations imposed a particularly stringent separation of spiking modes; here, we pharmacologically reduced or inactivated I_T through direct current injection to induce tonic spiking, while previous studies used ISI criteria to infer the presence of tonic spikes without experimental manipulation of I_T.

Burst Size Encoding of Low-Frequency Inputs

Decomposing ETA_{Burst} into slow ETA_{Ca} and fast ETA_{Na} features (Figure 3) revealed that events with different AP counts encoded distinct combinations of stimuli (Figure 3C) and, more causally, were driven by different levels of depolarization from the LTS (Figure 3D). Previous studies of model bursting neurons suggested that burst size may encode a variety of stimulus features (Elijah et al., 2015; Kepecs and Lisman, 2003; Kepecs et al., 2002), but this possibility had not been tested experimentally on at the single-neuron level. Our approach recalls the theoretical work of (Kepecs and Lisman, 2003) using covariance analysis. While both approaches find that events with different AP counts project to different regions of a reduced two-dimensional stimulus space, our dimensionality reduction approach identifies a temporal sequence of stimuli—a slow, biphasic oscillation followed by high-frequency excitation—rather than a combination of orthogonal stimulus features (Kepecs and Lisman, 2003). Moreover, we also observed that AP timing depended on high-frequency inputs, whereas Kepecs and Lisman (2003) reported that AP times within bursts were robust to noise. In general, it appears that models capturing the fast dynamics we observe experimentally are elusive, as we have not yet been able to reproduce high-frequency selectivity in standard bursting models (e.g., McCormick and Huguenard, 1992).

We found that current oscillations showing greater similarity to ETA_{Ca} evoked bursts with greater numbers of APs (Figure 3). The filtering properties of ETA_{Ca} capture thalamic sensitivity to slow background changes in membrane potential and large depolarizations which might arise from synchronous inputs, consistent with circuit-level observations in the visual thalamus. Butts et al. (2010) found that high spike count responses are evoked by stimuli more similar to the ETA; relatedly, Gaudry and Reinagel (2008) showed that burst size can encode sensory information and that larger bursts are preceded by stronger inhibitory stimuli, while Lesica et al. (2006) correlated the degree of inhibition present in the ETA with bursting in in vivo data and membrane potential in a model. Here, we directly show that the slow selectivity of ETA_{Ca} arises from I_T and that stimuli which best match this waveform trigger larger LTSs and bursts with more APs, linking stimulus encoding to the underlying bursting mechanism.

Encoding of the slow feature ETA_{Ca} depended on the overall statistical context of the stimulus, as changes in SD (σ) changed the fundamental forms of both the ETAs (Figure S5) and the corresponding IO relations (Figure 5) (see also Wolfart et al., 2005). This context sensitivity may arise because different σ values explore substantially different subthreshold voltage ranges, with different levels of I_T availability (Jahnsen and Llinás, 1984b). Indeed, our finding that slow s_{Ca} predicts LTS size (Figure 4D, inset) and the associated AP count supports a scenario where the low-frequency channel encodes the local σ in the number of APs per spiking event. This idea is consistent with the observed σ-dependent increase in burstiness (Figure S5). Conceptually, this finding is similar to how bursts can encode slope in a model neuron (Kepecs et al., 2002), albeit by an entirely different biophysical mechanism.

Adaptive Intraburst Encoding of High-Frequency Inputs

The most striking finding we report here is that during bursting and LTS generation, thalamic neurons remain selective for very fast inputs, enabling the AP times within bursts to accurately convey fine temporal details. This greatly increases the information content of thalamic bursts beyond "AP-count" codes where stimulus encoding is limited to the size of the burst (Lesica and Stanley, 2004; Gaudry and Reinagel, 2008; Elijah et al., 2015; Butts et al., 2010). Existing analyses of precise AP times within visually evoked thalamic bursts have not explored the role of specific stimulus selectivity within bursts, demonstrating rather that shorter initial ISIs in a burst are correlated with larger burst AP count (Gaudry and Reinagel, 2008) or duration (Butts et al., 2010), reflecting the fact that larger LTSs drive more APs separated by shorter intervals. In contrast, we show here that intraburst AP times can convey specific high-frequency information, distinct from burst size.

Encoding of high-frequency inputs showed gain scaling (Fairhall et al., 2001; Mease et al., 2013; Maravall et al., 2007), such that the information per AP was held constant regardless of stimulus contrast (Figure 5), as can arise from intrinsic spike generation in cortical neurons (Mease et al., 2013). Here, gain scaling is transiently gated by selectivity for low frequencies, as the LTS creates a window for adaptive encoding of fast features. Given the similar intrinsic properties of thalamic relay neurons across different nuclei and sensory systems (Jahnsen and Llinás, 1984a; Landisman and Connors, 2007), this fast encoding may be a generic scheme across levels of thalamic hierarchy (e.g., primary versus higher-order) and sensory modalities. For example, such a fast encoding channel may be an intrinsic mechanism supporting the extreme temporal precision of primary thalamic neurons' responses to whisker stimuli in vivo (Petersen et al., 2008).

Matching Synaptic Inputs to Intrinsic Computation

The multiplexed encoding we report is well matched to the variety of excitatory and inhibitory inputs that converge on thalamic relay neurons. Although the exact anatomical origin of inputs is nucleus specific, a general input scheme is the combination of fast "driver" and slow "modulatory" excitatory inputs of

brainstem and/or cortical origin, along with slow inhibitory inputs mainly from other thalamic nuclei (Sherman and Guillery, 2006). We used near-white-noise current to sample minimally biased models of feature selectivity (Rieke et al., 1997); this general thalamic input scheme predicts that the spectral properties of synaptic inputs to POm neurons in vivo likely favor high- and low-frequency inputs from different sources, as we detail below.

For POm neurons, these inputs are relatively well characterized and include inhibitory input from within the thalamus as well as modulatory excitatory input from cortical layer 6 (Reichova and Sherman, 2004; Mease et al., 2014; Crandall et al., 2015) and fast driving input from both the brainstem and cortical L5B (Groh et al., 2008, 2014; Reichova and Sherman, 2004; Mease et al., 2016c). In the multiplexing framework, inhibitory and layer 6 modulatory inputs could set the resting membrane potential and thereby control the availability of I_T and ETA shape (see also Lesica et al., 2006). L5B and brainstem inputs to POm are integrated within an ~50 ms window in vivo (Groh et al., 2014) and could provide the strong excitation needed to trigger an LTS; in this case, POm burst size may encode the degree of synchrony of L5B inputs (Groh et al., 2008) or the coincidence of L5B and brainstem inputs (Groh et al., 2014).

Stimuli triggering an LTS also "unlock" a fast encoding channel of transient sensitivity to high frequencies. Specific to POm, the timescales of ETA_{Tonic} and ETA_{Na} (Figures 2 and 4) correspond well to the fast rise (0.5 ms) and decay (1.2 ms) times of the glutamatergic "driver" excitatory postsynaptic currents (EPSCs) from cortical L5B (Groh et al., 2008), suggesting that POm's encoding of L5B inputs could also preserve fine L5B spiking structure, e.g., high-frequency bursts (de Kock and Sakmann, 2008). In fact, the LTS-dependent selectivity (Figure 4) and intrinsic adaptive gain control (Figure 5D) for high-frequency inputs may well match to the rapid synaptic gain control from short-term depression at L5B-POm synapses (Groh et al., 2008). Although these synapses depress strongly and rapidly, gain scaling could adjust thalamic excitability to normalize L5B input regardless of depression state. For example, the initial L5B spike would trigger large glutamate release at the L5B-POm synapse, thus activating I_T and the initiation of a POm LTS. Subsequent L5B spikes within the next ~50 ms would trigger only small EPSCs due to synaptic depression, but our results predict that such spikes could still induce additional POm APs during the transient window of enhanced high-frequency selectivity.

Implications for Circuit-Level Computations

The thalamus is an active and dynamic processor of information en route to the cortex. We find intrinsic properties alone allow thalamic neurons to (1) simultaneously transmit information on different timescales to the cortex, and (2) differentially adapt encoding of this information. In this multiplexed encoding scheme, the timing and size of bursts could reflect low-frequency input synchrony of the presynaptic network, while the timing of spikes could faithfully relay individual presynaptic spike times to the cortex. However, it remains an open question to what degree this information—particularly the fine-scale intraburst information—is indeed transmitted to the cortex and is relevant to sensory processing or behavior.

It is clear that thalamic bursts and single spikes evoke different responses in the cortex. Compared to single spikes, bursting strongly activates cortical networks (Swadlow and Gusev, 2001), evokes larger depolarizations in cortical neurons (Bruno and Sakmann, 2006), and promotes facilitation of cortical sensory responses (Whitmire et al., 2017). However, propagation of more precise burst *size* information requires that cortical responses scale with thalamic burst size, which has yet to be shown. One possible approach could be combining optogenetic methods with thalamic and cortical recordings (Whitmire et al., 2016; Mease et al., 2016a, 2016b; Whitmire et al., 2017).

The successful transmission of precise temporal information *within* bursts depends critically on the properties of thalamocortical (TC) connections. TC synapses from POm have submillisecond precision (~0.4 ms jitter) (Lee and Sherman, 2008), and the integration window of cortical neurons can be quite precise (1–10 ms) (Gabernet et al., 2005), suggesting that thalamic intraburst AP timing could in principle persist across the TC synapse. However, the AP-triggering efficacy of cortical excitatory postsynaptic potentials (EPSPs) corresponding to APs within a thalamic burst would be controlled by the depression or facilitation dynamics of the synapse. In the case of POm projections, these dynamics can be target-specific, as (Viaene et al., 2011) report both depressing and facilitating connections to primary and secondary somatosensory cortices, respectively. In the case of strong depression, survival of later thalamic spike times in cortex would likely be contingent on TC convergence onto single cortical neurons (Constantinople and Bruno, 2013; Bruno and Sakmann, 2006) and on strong, precise synchrony across thalamic neurons, which (Whitmire et al., 2016) find is promoted during bursting. Intriguingly, neurons in barrel cortex can encode separate channels of high- and low-frequency information about whisker displacement (Alenda et al., 2010), and our findings suggest that such parallel information streams are present at the level of single thalamic neurons.

EXPERIMENTAL PROCEDURES

Animal protocols followed the guidelines of German animal welfare and were approved by oversight committees at the Technische Universität München and Heidelberg University. In vivo recordings in 6- to 8-week-old thy1-ChR2 (line 18) or wild-type mice (both BL/6 background) of either sex were done as in Groh et al. (2014). In vitro whole-cell patch-clamp recordings were made in brain slices maintained at 33°C –35°C as described previously (Groh et al., 2008; Mease et al., 2013), for Wistar rats (n = 8 cells) and BL/6 mice (n = 8 cells) of either sex, 20–25 days after birth. Gaussian noise current stimuli were exponentially filtered with temporal correlation of 0.5 or 1.0 ms. We use "spiking event" to refer to a single AP or a burst of two or more APs. In the latter case, the time of the first AP is taken as the event time. Calculation of linear-nonlinear models was as described previously (Mease et al., 2013). ETA_{Burst} was split into components ETA_{Ca} and ETA_{Na} by fitting an exponential to the fast rising stimulus trajectory immediately preceding the trigger time (Figure S3). Details are found in Supplemental Experimental Procedures.

SUPPLEMENTAL INFORMATION

Supplemental Information includes Supplemental Experimental Procedures and five figures and can be found with this article online at http://dx.doi.org/10.1016/j.celrep.2017.04.050.

AUTHOR CONTRIBUTIONS

All authors contributed to research design and the final manuscript. R.A.M. and A.G. performed research, analyzed data, and wrote an initial draft of the manuscript.

ACKNOWLEDGMENTS

We thank Arthur Konnerth, Bert Sakmann, and Bernhard Meyer for lab space and support at the Technische Universität München. This work was funded by the DFG Collaborative Research Center (1158; R.A.M. and A.G.), the NIH (Institutional Grant for Neurobiology T32 GM07108–35), The Grass Foundation (R.A.M. and A.G.), the DFG Collaborative Research Center (1134) and CellNetworks Cluster of Excellence EXC 81 (T.K.), and the National Science Foundation (EF-0928251; A.L.F.).

Received: December 23, 2016
Revised: March 18, 2017
Accepted: April 18, 2017
Published: May 9, 2017

REFERENCES

Alenda, A., Molano-Mazón, M., Panzeri, S., and Maravall, M. (2010). Sensory input drives multiple intracellular information streams in somatosensory cortex. J. Neurosci. *30*, 10872–10884.

Alitto, H.J., Weyand, T.G., and Usrey, W.M. (2005). Distinct properties of stimulus-evoked bursts in the lateral geniculate nucleus. J. Neurosci. *25*, 514–523.

Bessaïh, T., Leresche, N., and Lambert, R.C. (2008). T current potentiation increases the occurrence and temporal fidelity of synaptically evoked burst firing in sensory thalamic neurons. Proc. Natl. Acad. Sci. USA *105*, 11376–11381.

Brenner, N., Strong, S.P., Koberle, R., Bialek, W., and de Ruyter van Steveninck, R.R. (2000). Synergy in a neural code. Neural Comput. *12*, 1531–1552.

Bruno, R.M., and Sakmann, B. (2006). Cortex is driven by weak but synchronously active thalamocortical synapses. Science *312*, 1622–1627.

Butts, D.A., Desbordes, G., Weng, C., Jin, J., Alonso, J.M., and Stanley, G.B. (2010). The episodic nature of spike trains in the early visual pathway. J. Neurophysiol. *104*, 3371–3387.

Coenen, A.M., and Vendrik, A.J. (1972). Determination of the transfer ratio of cat's geniculate neurons through quasi-intracellular recordings and the relation with the level of alertness. Exp. Brain Res. *14*, 227–242.

Constantinople, C.M., and Bruno, R.M. (2013). Deep cortical layers are activated directly by thalamus. Science *340*, 1591–1594.

Crandall, S.R., Cruikshank, S.J., and Connors, B.W. (2015). A corticothalamic switch: controlling the thalamus with dynamic synapses. Neuron *86*, 768–782.

de Boer, R., and Kuyper, P. (1968). Triggered correlation. IEEE Trans. Biomed. Eng. *15*, 169–179.

de Kock, C.P., and Sakmann, B. (2008). High frequency action potential bursts (>or= 100 Hz) in L2/3 and L5B thick tufted neurons in anaesthetized and awake rat primary somatosensory cortex. J. Physiol. *586*, 3353–3364.

Deleuze, C., David, F., Béhuret, S., Sadoc, G., Shin, H.S., Uebele, V.N., Renger, J.J., Lambert, R.C., Leresche, N., and Bal, T. (2012). T-type calcium channels consolidate tonic action potential output of thalamic neurons to neocortex. J. Neurosci. *32*, 12228–12236.

Denning, K.S., and Reinagel, P. (2005). Visual control of burst priming in the anesthetized lateral geniculate nucleus. J. Neurosci. *25*, 3531–3538.

Dreyfus, F.M., Tscherter, A., Errington, A.C., Renger, J.J., Shin, H.S., Uebele, V.N., Crunelli, V., Lambert, R.C., and Leresche, N. (2010). Selective T-type calcium channel block in thalamic neurons reveals channel redundancy and physiological impact of I(T)window. J. Neurosci. *30*, 99–109.

Elijah, D.H., Samengo, I., and Montemurro, M.A. (2015). Thalamic neuron models encode stimulus information by burst-size modulation. Front. Comput. Neurosci. *9*, 113.

Fairhall, A.L., Lewen, G.D., Bialek, W., and de Ruyter Van Steveninck, R.R. (2001). Efficiency and ambiguity in an adaptive neural code. Nature *412*, 787–792.

Fairhall, A.L., Burlingame, C.A., Narasimhan, R., Harris, R.A., Puchalla, J.L., and Berry, M.J., 2nd. (2006). Selectivity for multiple stimulus features in retinal ganglion cells. J. Neurophysiol. *96*, 2724–2738.

Fanselow, E.E., Sameshima, K., Baccala, L.A., and Nicolelis, M.A. (2001). Thalamic bursting in rats during different awake behavioral states. Proc. Natl. Acad. Sci. USA *98*, 15330–15335.

Gabernet, L., Jadhav, S.P., Feldman, D.E., Carandini, M., and Scanziani, M. (2005). Somatosensory integration controlled by dynamic thalamocortical feed-forward inhibition. Neuron *48*, 315–327.

Gaudry, K.S., and Reinagel, P. (2008). Information measure for analyzing specific spiking patterns and applications to LGN bursts. Network *19*, 69–94.

Groh, A., de Kock, C.P., Wimmer, V.C., Sakmann, B., and Kuner, T. (2008). Driver or coincidence detector: modal switch of a corticothalamic giant synapse controlled by spontaneous activity and short-term depression. J. Neurosci. *28*, 9652–9663.

Groh, A., Bokor, H., Mease, R.A., Plattner, V.M., Hangya, B., Stroh, A., Deschenes, M., and Acsady, L. (2014). Convergence of cortical and sensory driver inputs on single thalamocortical cells. Cereb. Cortex *24*, 3167–3179.

Guido, W., and Weyand, T. (1995). Burst responses in thalamic relay cells of the awake behaving cat. J. Neurophysiol. *74*, 1782–1786.

Jahnsen, H., and Llinás, R. (1984a). Electrophysiological properties of guinea-pig thalamic neurones: an in vitro study. J. Physiol. *349*, 205–226.

Jahnsen, H., and Llinás, R. (1984b). Ionic basis for the electro-responsiveness and oscillatory properties of guinea-pig thalamic neurones in vitro. J. Physiol. *349*, 227–247.

Kepecs, A., and Lisman, J. (2003). Information encoding and computation with spikes and bursts. Network *14*, 103–118.

Kepecs, A., Wang, X.-J., and Lisman, J. (2002). Bursting neurons signal input slope. J. Neurosci. *22*, 9053–9062.

Korenberg, M.J., and Hunter, I.W. (1986). The identification of nonlinear biological systems: LNL cascade models. Biol. Cybern. *55*, 125–134.

Lambert, R.C., Bessaih, T., Crunelli, V., and Leresche, N. (2014). The many faces of T-type calcium channels. Pflugers Arch. *466*, 415–423.

Landisman, C.E., and Connors, B.W. (2007). VPM and PoM nuclei of the rat somatosensory thalamus: intrinsic neuronal properties and corticothalamic feedback. Cereb. Cortex *17*, 2853–2865.

Lee, C.C., and Sherman, S.M. (2008). Synaptic properties of thalamic and intracortical inputs to layer 4 of the first- and higher-order cortical areas in the auditory and somatosensory systems. J. Neurophysiol. *100*, 317–326.

Lesica, N.A., and Stanley, G.B. (2004). Encoding of natural scene movies by tonic and burst spikes in the lateral geniculate nucleus. J. Neurosci. *24*, 10731–10740.

Lesica, N.A., Weng, C., Jin, J., Yeh, C.I., Alonso, J.M., and Stanley, G.B. (2006). Dynamic encoding of natural luminance sequences by LGN bursts. PLoS Biol. *4*, e209.

Lesica, N.A., Jin, J., Weng, C., Yeh, C.I., Butts, D.A., Stanley, G.B., and Alonso, J.M. (2007). Adaptation to stimulus contrast and correlations during natural visual stimulation. Neuron *55*, 479–491.

Livingstone, M.S., and Hubel, D.H. (1981). Effects of sleep and arousal on the processing of visual information in the cat. Nature *291*, 554–561.

Llinás, R.R., and Steriade, M. (2006). Bursting of thalamic neurons and states of vigilance. J. Neurophysiol. *95*, 3297–3308.

Maravall, M., Petersen, R.S., Fairhall, A.L., Arabzadeh, E., and Diamond, M.E. (2007). Shifts in coding properties and maintenance of information transmission during adaptation in barrel cortex. PLoS Biol. *5*, e19.

Maravall, M., Alenda, A., Bale, M.R., and Petersen, R.S. (2013). Transformation of adaptation and gain rescaling along the whisker sensory pathway. PLoS ONE *8*, e82418.

Martinez-Conde, S., Macknik, S.L., and Hubel, D.H. (2002). The function of bursts of spikes during visual fixation in the awake primate lateral geniculate nucleus and primary visual cortex. Proc. Natl. Acad. Sci. USA *99*, 13920–13925.

McCormick, D.A., and Huguenard, J.R. (1992). A model of the electrophysiological properties of thalamocortical relay neurons. J. Neurophysiol. *68*, 1384–1400.

Mease, R.A., Famulare, M., Gjorgjieva, J., Moody, W.J., and Fairhall, A.L. (2013). Emergence of adaptive computation by single neurons in the developing cortex. J. Neurosci. *33*, 12154–12170.

Mease, R.A., Krieger, P., and Groh, A. (2014). Cortical control of adaptation and sensory relay mode in the thalamus. Proc. Natl. Acad. Sci. USA *111*, 6798–6803.

Mease, R.A., Metz, M., and Groh, A. (2016a). Cortical sensory responses are enhanced by the higher-order thalamus. Cell Rep. *14*, 208–215.

Mease, R.A., Sumser, A., Sakmann, B., and Groh, A. (2016b). Cortical dependence of whisker responses in posterior medial thalamus in vivo. Cereb. Cortex *26*, 3534–3543.

Mease, R.A., Sumser, A., Sakmann, B., and Groh, A. (2016c). Corticothalamic spike transfer via the L5B-POm pathway in vivo. Cereb. Cortex *26*, 3461–3475.

Panzeri, S., Brunel, N., Logothetis, N.K., and Kayser, C. (2010). Sensory neural codes using multiplexed temporal scales. Trends Neurosci. *33*, 111–120.

Petersen, R.S., Brambilla, M., Bale, M.R., Alenda, A., Panzeri, S., Montemurro, M.A., and Maravall, M. (2008). Diverse and temporally precise kinetic feature selectivity in the VPm thalamic nucleus. Neuron *60*, 890–903.

Ramcharan, E.J., Gnadt, J.W., and Sherman, S.M. (2000). Burst and tonic firing in thalamic cells of unanesthetized, behaving monkeys. Vis. Neurosci. *17*, 55–62.

Reichova, I., and Sherman, S.M. (2004). Somatosensory corticothalamic projections: distinguishing drivers from modulators. J. Neurophysiol. *92*, 2185–2197.

Reinagel, P., Godwin, D., Sherman, S.M., and Koch, C. (1999). Encoding of visual information by LGN bursts. J. Neurophysiol. *81*, 2558–2569.

Rieke, F., Warland, D., de Ruyter van Steveninck, R.R., and Bialek, W. (1997). Spikes: Exploring the Neural Code (MIT Press).

Senatore, A., Zhorov, B.S., and Spafford, J.D. (2012). Cav3 T-type calcium channels. Wiley Interdiscip. Rev. Membr. Transp. Signal. *1*, 467–491.

Shannon, C.E., and Weaver, W. (1963). The Mathematical Theory of Communication (University of Illinois Press).

Sherman, S.M. (2001). Tonic and burst firing: dual modes of thalamocortical relay. Trends Neurosci. *24*, 122–126.

Sherman, S.M., and Guillery, R. (2006). Exploring the Thalamus and Its Role in Cortical Function (MIT Press).

Simons, D.J., and Carvell, G.E. (1989). Thalamocortical response transformation in the rat vibrissa/barrel system. J. Neurophysiol. *61*, 311–330.

Swadlow, H.A., and Gusev, A.G. (2001). The impact of 'bursting' thalamic impulses at a neocortical synapse. Nat. Neurosci. *4*, 402–408.

Viaene, A.N., Petrof, I., and Sherman, S.M. (2011). Properties of the thalamic projection from the posterior medial nucleus to primary and secondary somatosensory cortices in the mouse. Proc. Natl. Acad. Sci. USA *108*, 18156–18161.

Wang, X., Wei, Y., Vaingankar, V., Wang, Q., Koepsell, K., Sommer, F.T., and Hirsch, J.A. (2007). Feedforward excitation and inhibition evoke dual modes of firing in the cat's visual thalamus during naturalistic viewing. Neuron *55*, 465–478.

Weyand, T.G., Boudreaux, M., and Guido, W. (2001). Burst and tonic response modes in thalamic neurons during sleep and wakefulness. J. Neurophysiol. *85*, 1107–1118.

Whitmire, C.J., Waiblinger, C., Schwarz, C., and Stanley, G.B. (2016). Information coding through adaptive gating of synchronized thalamic bursting. Cell Rep. *14*, 795–807.

Whitmire, C.J., Millard, D.C., and Stanley, G.B. (2017). Thalamic state control of cortical paired-pulse dynamics. J. Neurophysiol. *117*, 163–177.

Wolfart, J., Debay, D., Le Masson, G., Destexhe, A., and Bal, T. (2005). Synaptic background activity controls spike transfer from thalamus to cortex. Nat. Neurosci. *8*, 1760–1767.

Zeldenrust, F., Chameau, P.J., and Wadman, W.J. (2013). Reliability of spike and burst firing in thalamocortical relay cells. J. Comput. Neurosci. *35*, 317–334.